

This is a non-peer-reviewed preprint submitted to EarthArXiv.

This manuscript has been submitted for publication in Geophysical Research Letters. Please note the manuscript has yet to be formally accepted for publication. Subsequent versions of this manuscript may have slightly different content. If accepted, the final version of this manuscript will be available via the 'Peer-reviewed Publication DOI' link on the right-hand side of this webpage. Please feel free to contact any of the authors; we welcome feedback.

- 1 Barrier vulnerability following outwash: A balance of overwash and dune gap recovery
- 2 A. G. Van Blunk<sup>1</sup>, K. A. Anarde<sup>1</sup>, A. B. Murray<sup>2</sup>, L. J. Moore<sup>3</sup>, C. R. Sherwood<sup>4</sup>
- <sup>1</sup>Department of Civil, Construction, and Environmental Engineering, North Carolina State
- 4 University, Raleigh, NC, USA.
- 5 <sup>2</sup>Division of Earth and Climate Sciences, Nicholas School of the Environment, Duke University,
- 6 Durham, NC, USA.
- 7 <sup>3</sup>Department of Earth, Marine and Environmental Sciences, University of North Carolina at
- 8 Chapel Hill, Chapel Hill, NC, USA.
- <sup>4</sup>Woods Hole Coastal and Marine Science Center, U.S. Geological Survey, Woods Hole, MA, USA.
- 11 Corresponding author: Katherine Anarde (<u>kanarde@ncsu.edu</u>)

### 13 **Key Points:**

10

- Simulations of outwash events reduce the height and width of barriers for decades after an event.
- When modeled outwashed sand stays nearshore, it can supply the material needed for
   dune growth while also buffering shoreline erosion.
- Faster dune growth closes gaps sooner, reducing vulnerability to future outwash events,
   but limiting interior recovery via overwash.

### **Abstract**

Existing barrier evolution models only simulate storm impacts from landward-driven flows (overwash), neglecting the impacts of seaward-directed flows (outwash). Here, we modify an existing model to incorporate outwash processes. We find that outwash enhances barrier vulnerability (the tendency to drown) over decadal timescales by scarring the island interior, creating lower, narrower landforms. If outwashed sand stays nearshore, a wider beach and steeper shoreface facilitate dune recovery and closure of gaps, which are otherwise maintained by overwash. Importantly, faster (natural) dune growth means the barrier is less vulnerable to future outwash events, but potentially more vulnerable to back-barrier drowning from sea-level rise because dunes also limit building of interior elevation by overwash. Any changes in storm climatology could alter the balance between dune recovery and overwash making the future vulnerability of modern outwashed barriers difficult to assess.

#### Plain Language Summary

Bay-to-ocean flows have been observed to erode barrier islands backed by large bays or sounds, creating channels through gaps in the dunes. Here we use a model to show that factors that influence the closing of dune gaps are particularly important for barrier island resilience to future storm events and sea-level rise. If sediment eroded during outwash stays close to shore, it creates a wider beach, which gives dunes a chance to grow and fill gaps. Closure of dune gaps limits preferential pathways for flow driven by elevated bayside water levels during subsequent storm events. But there is a tradeoff: if the dunes grow too fast, they prevent any recovery of the barrier island interior from sand deposited by ocean-to-bay flows. This results in barrier islands with tall dunes, but lower and narrower interiors that are susceptible to inundation by sea-level rise.

#### 1 Introduction

Barrier islands, spits, and peninsulas ('barriers') are dynamic coastal landforms that change shape in response to storm, climatic, and human processes over a range of spatial and temporal scales. During storms, elevated oceanside water levels can overtop dunes and transport sediment eroded from the front of the barrier system – including the shoreface, beach, and

48 dunes – to the barrier interior and back bay (Dolan & Godfrey, 1973; Donnelly et al., 2006). This 49 landward flux of water and sediment, called "overwash", results in "washover" deposits (Figure 50 1a). Washover facilitates island migration (Leatherman, 1979), and the elevation gained allows 51 barrier systems to keep pace with sea-level rise (SLR) (Kochel & Dolan, 1986). 52 Observations show that "outwash" (seaward-directed flows) can produce significant 53 morphological change across barrier systems backed by large bays(Hayes, 1967; Wright et al., 54 1970). Outwash occurs when offshore-directed winds increase bay-side water levels, creating a 55 gradient that drive flow across a barrier from the bay to the ocean (Anarde et al., 2020; Bush & 56 Pilkey, 1994; Goff et al., 2010, 2019; Hall et al., 1990; Lennon, 1991; Over et al., 2021; Sherwood et al., 2014). These generate erosional "washout" features (e.g., channels and wide 57 58 dune gaps; Figure 1b), carrying sediment to the ocean. Sediment loss can be significant: after 59 Hurricane Dorian, 86 washout channels were carved into North Core Banks (NCB) in North 60 Carolina, resulting in an 18% barrier volume loss (Over et al., 2021; Sherwood et al., 2023). 61 Outwash occurs less frequently than overwash, but the scale of morphological changes likely 62 affect barrier evolution (Over et al., 2021, Sherwood et al., 2023). Observations of landscape 63 change by outwash have focused on short-term impacts (~1 year: Gayes 1991; Goff et al., 2010, 64 2019; Hall et al., 1990; Hayes, 1967; Lennon, 1991; Over et al., 2021; Sherwood et al., 2023; 65 Wright et al., 1970). Longer term studies (years to decades) are limited and focus on the barrier 66 interior (Himmelstein & Rodriguez, 2025; Over & Sherwood, 2025), which recovers slowly. 67 Multi-year observations of former washout channels in Texas, North Carolina, and New York 68 show that revegetation occurs slower than at washover sites, presumably because all organic 69 material, including seeds and rhizomes, are stripped out during outwash, and the channels 70 subsequently filled with relatively sterile marine sands (Over & Sherwood, 2025). The lack of 71 vegetation hinders dune formation (Durán and Moore, 2013; Hesp, 1989; Zarnetske et al., 72 2012), so the former outwash sites remain low and vulnerable to overwash (Over & Sherwood, 73 2025). 74 The fate of washed out sand is largely unknown and may vary based on the event or coastal 75 setting. Models of NCB (Warner et al., 2025) indicate deposition in the nearshore, but if 76 washout is lost from the cross-shore sediment budget (Goff et al., 2010), there may not be

77	enough overwashing sediment for recovery of the barrier interior, and the barrier could drown
78	(Anarde et al., 2024a; Lorenzo-Trueba & Ashton, 2014; Moore et al., 2010). Additionally, any
79	changes to the equilibrium shoreface shape from washout may influence barrier migration
80	(e.g., Ashton and Ortiz, 2011; Lorenzo-Trueba & Ashton, 2014).
81	Previously developed models of long-term barrier evolution (e.g., Anarde et al., 2024a; Lorenzo-
82	Trueba & Ashton, 2014; Moore et al., 2010; Nienhuis & Lorenzo-Trueba, 2019; Reeves et al.,
83	2021) do not include outwash dynamics. In this study we explore the role that outwash plays in
84	barrier evolution, building on an existing "synthesist" (French et al., 2016) barrier evolution
85	model (Anarde et al., 2024a), calibrated with recorded washout features.
86	2 Implementing Outwash in CASCADE
87	The CoAStal Community-IAnDscape Evolution (CASCADE) model is a coupled modeling
88	framework that simulates natural and human-modified barrier evolution (Anarde et al., 2023,
89	2024a). Barrier3D (Reeves et al., 2021) is the core of CASCADE, incorporating SLR, dune
90	dynamics, overwash, and shoreface adjustments. Barrier3D can be coupled to other models
91	(e.g., BRIE; Nienhuis & Lorenzo Trueba, 2019) and modules within CASCADE. Here, we introduce
92	a new module that simulates outwash on natural barriers. In the following sections, we
93	describe the parameterization of outwash within CASCADE. For a complete description of
94	model processes beyond outwash, the reader is directed to Anarde et al. (2024a) and Reeves et
95	al. (2021).
96	2.1 Flow routing and sediment transport
97	The core morphological feature of the outwash module is a cellular flow routing algorithm
98	(Murray & Paola, 1994, 1997), first modified to simulate overwash (Reeves et al., 2021), and
99	here modified to simulate outwash. The equations and algorithm are described in detail in the
100	supplement (Text S1) and summarized below.
101	In CASCADE, the dune and barrier interior are treated separately with different dynamics
102	(Reeves et al., 2021). For simulation of outwash, we merge the dune and interior domains and
103	route flow and sediment from the interior across the barrier toward the ocean. Additionally, we

104	add a beach domain to better replicate water-level slopes shown to drive morphological change
105	during outwash (e.g., Sherwood et al., 2014, 2023; Warner et al., 2025). This representation of
106	the beach domain is used only to force dune and interior morphology change during storms:
107	beach change does not carry over between CASCADE model years and resets prior to every new
108	outwash event. A different beach domain is used as a buffer for shoreface dynamics after an
109	outwash event (see below).
110	Flow and sediment transport parameters were tuned to best match observed washout features
111	from Hurricane Dorian on NCB (Figure 1). Pre-storm dune crest heights along this section of
112	NCB averaged 3.3 m mean high water (MHW; Figure 1). The black, purple, and blue outlined
113	pre-storm domains ("configurations 1, 2, and 3", respectively) were used to tune the model
114	parameters to best match washout volumes and morphologies identified using the post-storm
115	domains (Figure S4). The orange outlined domain ("configuration 4") was used for model
116	testing (Figure S5). All results discussed in this study (Section 4) use pre-storm configuration 4.
117	We use an hourly hydrograph from the ADvanced CIRCulation Model (ADCIRC; Westerink et al.,
118	1992) as the hydrodynamic forcing of bay-side water elevations to simulate Hurricane Dorian
119	(Sherwood et al., 2023; Text S1 and Figure S2).

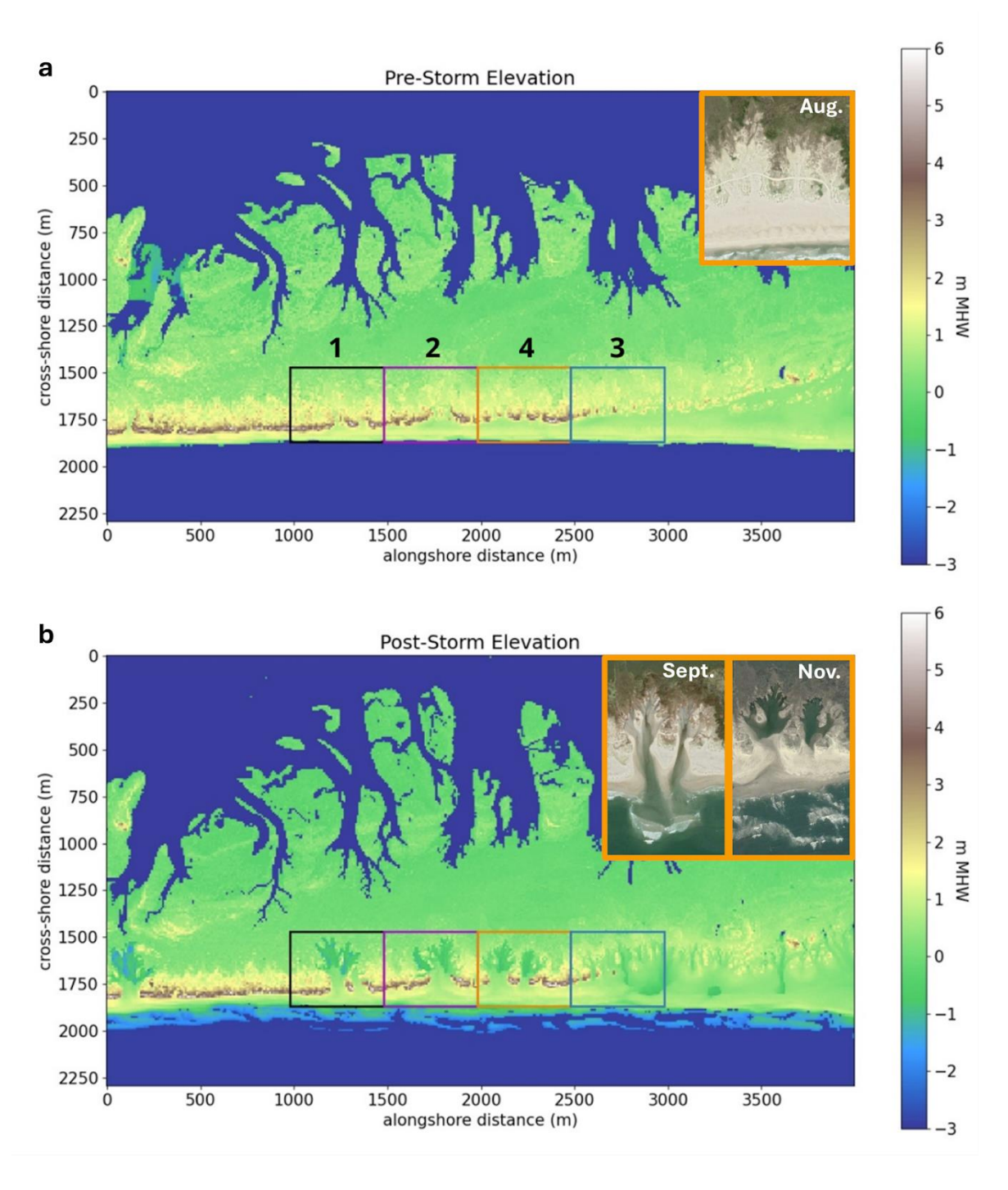


**Figure 1**. Elevation map with four domains used in model development and simulations (a) two years before and (b) weeks to months after Hurricane Dorian (2019) along North Core Banks, North Carolina. The black, purple, and blue domains ("configurations 1, 2, and 3", respectively) were used for model tuning while the orange domain ("configuration 4") was used for model testing. The pre-storm aerial image in (a) depicts overwash fans in August 2019, one month

126 before Hurricane Dorian. The two post-storm aerial images in (b) show washout channels days 127 after Hurricane Dorian, and subsequent infilling of those channels two months later. 128 2.2 Lateral dune erosion 129 Sediment is transported laterally (in the alongshore direction) between neighboring cells when 130 submerged by outwash. The lateral sediment transport is proportional to the lateral slope and 131 the total downstream sediment flux (Parker, 1978). Therefore, submerged cells at the edge of 132 dune gaps receive sediment from higher, neighboring dune cells. This lowers the neighboring 133 dune cell and widens the dune gap. 134 2.3 Shoreface incorporation of washout 135 Once sediment has been routed across the barrier, some or all of it is incorporated into the 136 shoreface, similar to how beach nourishment is simulated in CASCADE (Anarde et al., 2024a). 137 We distribute sediment along both the upper and lower shoreface, which shifts the shoreline 138 seaward and steepens the shoreface slope, as the shoreface toe remains fixed. The cross-shore 139 location of the dune line is fixed, so a more seaward shoreline position creates a beach that 140 carries between model years (separate from the beach domain discussed in Section 2.1). Here, 141 the beach acts as a buffer to (post-storm) shoreline erosion, like the washout deltas observed 142 by Sherwood et al. (2023) (Figure 1b). If the beach completely erodes in subsequent model 143 years, landward migration of the dune line recommences. 144 **3 Initial Conditions and Model Scenarios** 145 We assess the long-term impact of outwash on barrier dynamics by examining sensitivity to 146 both subaqueous and subaerial factors, including 1) the degree to which washout is 147 incorporated into the shoreface, and 2) how quickly dunes recover following an outwash 148 event. 149 We test three scenarios for washout incorporation into the shoreface: 100% (all sediment 150 remains in the cross-shore system), 50% (half remains), and 0% (all is lost). The 0% scenario is 151 used to differentiate between the subaerial impacts of outwash (erosion of the barrier interior

and dunes) and evolutionary changes driven by shoreface dynamics (subaqueous impacts).

153 We test two scenarios for dune recovery. The dune growth rate r controls the shape of the 154 logistic growth curve (Durán and Moore, 2013; Houser et al., 2015): we use r = 0.25 as a low 155 dune growth rate and r = 0.35 as a slightly higher dune growth rate. In the model, dunes grow 156 up to a maximum elevation (Durán Vinent & Moore, 2015), here set to 6.2 m MHW (the largest 157 value across the NCB domain). 158 To represent overwash as a function of storm stochasticity and dune height, which varies 159 throughout time ("dune-storm stochasticity"; Anarde et al., 2024), we run each scenario with 160 100 different storm sequences, each 100 years long (allowing multiple storms in a single model 161 year, all occurring from high ocean-side water levels). These ocean-side storm series are 162 parameterized for NCB using the multivariate method of Wahl et al., (2016), as in Reeves et al. 163 (2021) and Anarde et al. (2024a). Although we account for stochasticity in ocean-side storms, 164 we do not account for variability in the duration, magnitude, or incidence of outwash storms 165 (i.e., external forcing) because our focus is on the evolutionary behavior that stems from 166 differences in dune and shoreface dynamics (i.e., internal forcing). Instead, we simulate a single 167 outwash storm (Section 2.1, Figure S2) every 20 years (i.e., at model years 1, 21, 41, 61, and 168 81). However, outwash only occurs at these intervals if elevated bay-side water levels can 169 overtop dune gaps. If a model year has both ocean-side and outwash storms, the ocean-side 170 storm series is simulated before the outwash storm. 171 Lastly, if a barrier becomes too low or narrow in CASCADE, it will drown. Barrier transitions 172 from submerged to subaerial states (e.g., Mariotti and Hein, 2022) are not included here: if 173 drowning occurs, the simulation stops. 174 Below, we call simulations that incorporate different washout scenarios and dune growth rates 175 the "outwash scenarios" and compare them to a "baseline" scenario that simulates the same 176 storm sequences without outwash. 177 4 Results 178 Measures of barrier vulnerability (percent drowned), storm sediment fluxes (outwash and 179 overwash), dune dynamics (dune crest elevation and total length of dune gaps), and barrier

evolution (final interior elevation, final interior width, and final shoreline position) are

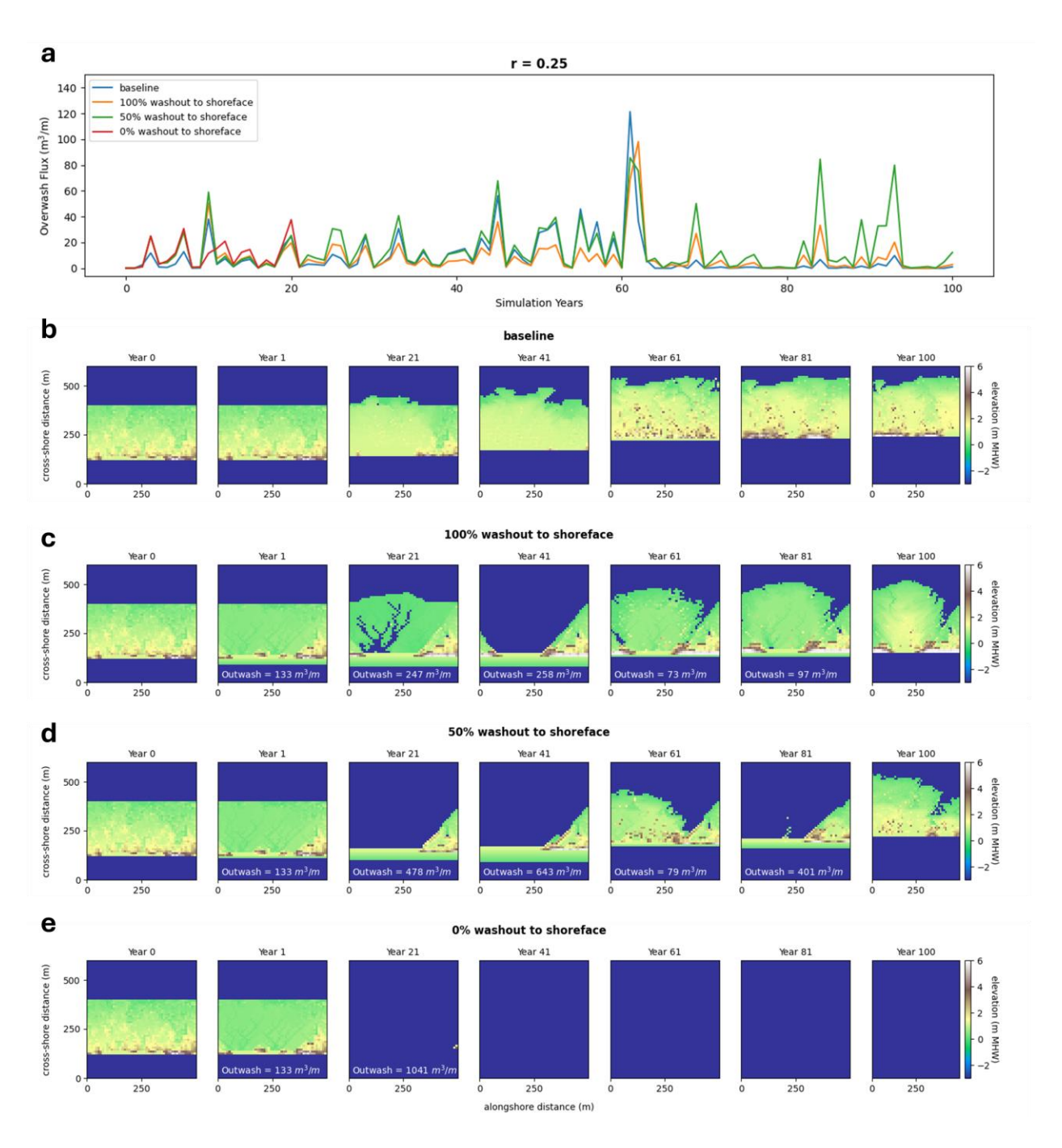
compared for each outwash and dune-growth scenario and then averaged across all 100 storm
sequences (Table 1). Percent drowned represents the number of barriers that drown before
reaching the 100 <sup>th</sup> model year. Average final shoreline position is the net migration averaged
across all runs in which drowning does not occur. The supplement contains more details on
how we calculated each variable (Text S1).

Table 1. Average measures of barrier morphology and migration for 100 storm sequences for eight scenarios, including baseline,
 outwash (100%, 50%, and 0% of the washout incorporated into the shoreface) scenarios, and two dune growth rates (*r* = 0.25 and
 0.35).

		r = 0.25									r = 0.35							
Scenarios	% drown ed	Overwas h Flux (m³/m/yr )	Outwash Flux (m³/m/yr )	Dune Crest Elevation (m MHW)	Total Length of Dune Gaps (m)	Final Interior Elevation (m MHW)	Final Interior Width (m)	Final Shoreline Position (m)	% drown ed	Overwas h Flux (m³/m/yr )	Outwash Flux (m³/m/yr )	Dune Crest Elevation (m MHW)	Total Length of Dune Gaps (m)	Final Interior Elevation (m MHW)	Final Interior Width (m)	Final Shoreline Position (m)		
		Mean	Mean	Mean	Mean	Mean	Mean	Mean		Mean	Mean	Mean	Mean	Mean	Mean	Mean		
Baseline	0	11	-	1.20	262	0.98	298	139	0	9	-	1.66	207	0.92	275	130		
100% Washout to Shoreface	15	14	361	2.06	223	0.62	198	10	5	8	232	3.00	125	0.75	153	27		
50% Washout to Shoreface	62	17	512	1.39	322	0.63	166	94	42	13	407	2.06	243	0.60	133	81		
0% Washout to Shoreface	89	17	542	1.10	392	0.67	155	127	83	16	519	1.34	367	0.73	110	172		

### 4.1 Sensitivity to Washout Incorporation into the Shoreface

We use the low dune-growth rate (r = 0.25) simulations to assess the effect of washout incorporation on barrier recovery. None of the barriers drown (Table 1) in the baseline scenario, despite a narrow (< 500 m) and low-lying (< 2 m MHW) initial barrier (Figure 2b, Year 0). In this case, overwash delivery to the barrier interior is sufficient for the barrier to keep pace with SLR, as illustrated for a single storm sequence (Figure 2a). In contrast, barrier drowning is more likely in the outwash scenarios, and the likelihood of drowning increases as more sediment is lost from the cross-shore system: 15%, 62%, and 89% of barriers drown when all, half, or none of the washout is incorporated into the shoreface, respectively (Table 1). The average increase in overwash flux for the outwash scenarios compared to baseline (Table 1), is insufficient to counter outwash losses and maintain barrier elevation and width (e.g., Figure 2c-e). So, while outwash can enhance overwash fluxes, on balance, barrier vulnerability increases for all washout scenarios because the barrier interior erodes (outwash flux, Table 1 and Figure 2c-e). Collectively, outwash results in barriers with lower average elevations (0.62-0.67 m MHW) and narrower widths (155-198 m) after 100 model years, compared to baseline (0.98 m MHW and 298 m, respectively; Table 1).



**Figure 2. a)** Overwash flux and **b-e)** barrier island elevation plan views for the low-dune-growth-rate scenario (r = 0.25) for a single storm sequence. Plan views are limited to outwash events (every 20 years) plus the initial (year 0) and final (year 100) elevations. Outwash fluxes are included on the plan views when relevant.

Feedbacks between shoreface and dune dynamics also influence barrier evolution following
outwash. These are best illustrated by individual simulations (Figure 2). In the model, more
washout on the shoreface leads to wider beaches (e.g., Figure 2c-d, Year 1), as illustrated by
shoreline position (Figure 3a). After the initial outwash event, the pattern of shoreline retreat
and barrier migration varies with the outwash scenario. For the 100% and 50% scenarios, as sea
level rises, the beach (and shoreline) erodes; overwash also harvests sediment from the upper
shoreface, resulting in landward migration of the shoreline. The dunes are immobile in the
model until the beach that separates the shoreline from the dunes fully erodes. The time series
of average dune-crest elevations (Figure 3b) demonstrates that for the 100% scenario, dunes
never migrate landward because a wide beach persists (Figure 2c and 3a). In contrast, without
the beach buffer generated through washout, dunes in the baseline scenario migrate landward
with the shoreline as illustrated by the increase in dune elevation at Year 60 (Figure 3b). While
Figures 2 and 3 illustrate the dynamics associated with a single 100-year overwash storm
sequence, Table 1 shows that the buffering effect of the washout-generated beach on dune and
shoreline migration is consistent across the 100 simulations: the average final shoreline
position for the baseline scenario is 139 m versus 10 m and 94 m for the 100% and 50%
scenarios, respectively.
beach buffer created by washout also gives dunes more time to grow while the beach erodes.
Hence, in the model, sediment that stays nearshore (100% and 50% scenarios) aids in dune
recovery, and on average, results in higher dune-crest elevations (2.06 and 1.39 m MHW,
respectively) compared to baseline (1.20 m MHW; Table 1). However, dune growth is not
spatially homogeneous. Figure 3b shows that dune gaps, which were pre-existing at the start of
the model simulations (100 m in total length) persist in all washout scenarios. In the model,
dune gaps can narrow or close through lateral sediment transport from higher to lower dunes.
For the storm sequence and dune growth rate in Figure 3b, dune gaps do not close under any
scenario, but they narrow in the 100% scenario. This trend is consistent across all 100
simulations (Table 1): on average, while the total length of dune gaps increases for the 0% and
50% scenarios (392 and 322 m, respectively) beyond baseline (262 m), the 100% scenario yields
narrowing dune gaps (223 m).

The 0% scenario does not provide any buffer between shoreline and dune erosion. Therefore, the outwash event at year 1, which causes significant subaerial erosion to the barrier interior, is followed by persistently low dunes and wider dune gaps (Table 1 and Figure 3b). While washover begins to rebuild the barrier interior, for the storm sequence in Figures 2-3, the barrier interior remains low and narrow by the second outwash event at year 21, after which the barrier drowns. Below, we elaborate on how faster dune gap recovery (via higher dune growth rates) can increase barrier resilience to drowning from sequential outwash events.

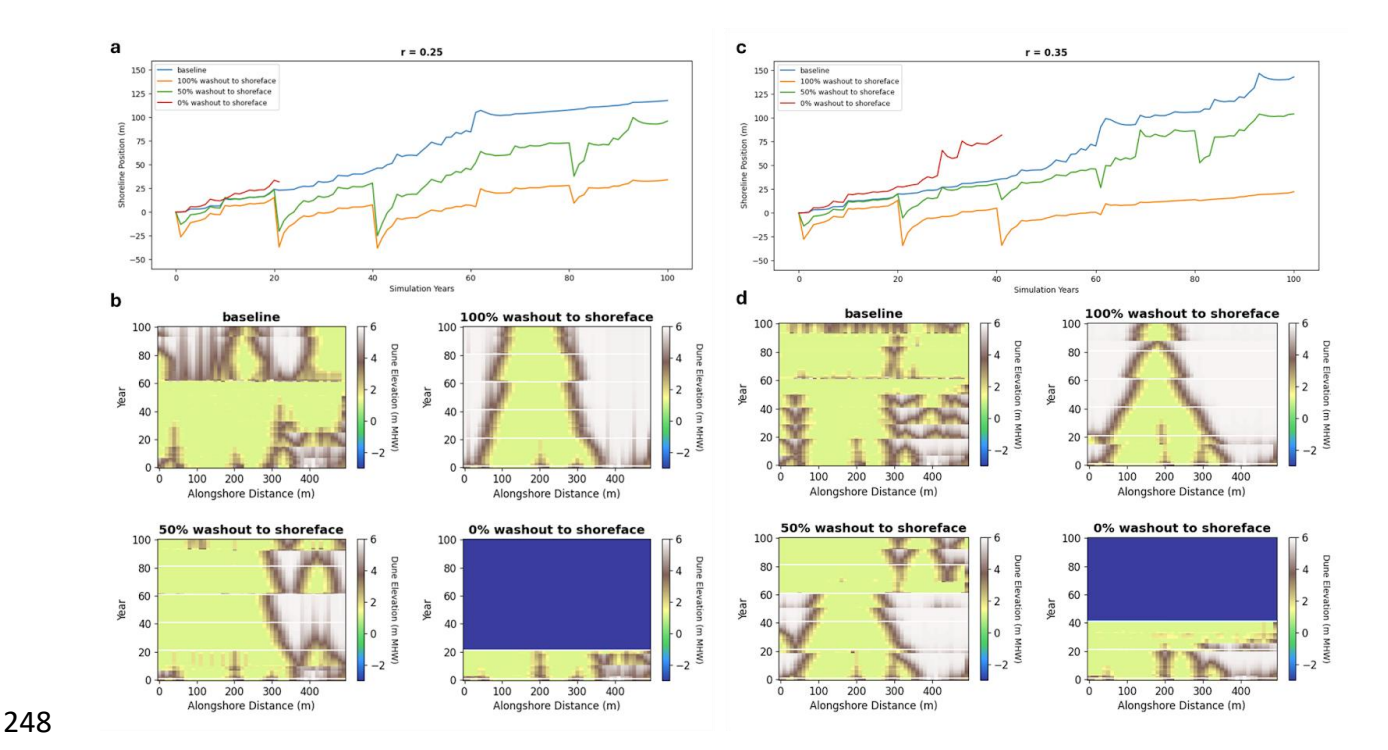


**Figure 3. a, c)** Shoreline position and **b, d)** dune elevation for the same storm sequence shown in Figure 2. The shoreline position only shows migration until a barrier drowns. Similarly, if a barrier drowns, the dune elevation in **b, d)** is set to -3 m MHW to represent water. The horizontal white lines on the dune elevation time series depict outwash event years.

### 4.2 Sensitivity to dune growth

Barriers with higher dune growth rates are less likely to drown in our simulations (6-20% reduction) because the higher dune growth rate leads to narrower dune gaps, which feeds back to limit outwash fluxes for subsequent storms (Table 1). A small increase in dune growth rate allows for faster narrowing and infilling of dune gaps as a simulation progresses (compare

Figure 3d (r = 0.35) with 3b (r = 0.25)). At Years 21 and 41, the dune gaps are clearly narrower for the higher dune growth rate, leading to a decrease in outwash flux at those years for all outwash scenarios (Figure S6). The fate of washout alters patterns of dune recovery, as discussed previously for low dune growth rates. At high dune growth rates, the average total length of dune gaps increases with the 0% (367 m) and 50% (243 m) scenarios compared to baseline (207 m) but decreases in the 100% (125 m) scenario because the large beach buffer allows dune gaps to recover. On average, the 100% scenario has the lowest outwash sediment fluxes but the largest percent reduction in outwash fluxes between the dune growth rates (36% reduction; Table 1), followed by the 50% and 0% scenarios (21% and 4% reduction, respectfully). Hence, the shoreface-dune growth coupling that stems from washout incorporation into the shoreface enhances this second coupling whereby faster dune recovery in gaps reduces subsequent outwash fluxes. Although taller, faster growing dunes decrease the destructive potential of subsequent outwash events by narrowing dune gaps and reduce the probability of barrier drowning, dune recovery also limits overwash to the barrier interior (Table 1 and Figure S6c-e). For outwash simulations that do not result in barrier drowning, the barriers are narrower with higher dune growth rates (110-153 m) than with lower dune growth rates (155-198 m), although average interior elevations are comparable (Table 1).

### **5 Discussion and Conclusions**

258

259

260

261

262

263

264

265

266

267

268

269

270

271

272

273

274

275

276

277

278

279

280

281

282

283

284

Our model shows that outwash enhances barrier island vulnerability through an increased tendency for barriers to drown (Table 1). This is driven by erosional scarring of the barrier interior as bay-to-ocean flows are funneled through dune gaps (Figure 2). Recovery of the barrier interior relies on overwash through dune gaps, but overwash also keeps dune gaps low and wide, making the barrier vulnerable to further erosion from outwash events (e.g., for the 0% washout to shoreface scenario in Figure 3b, d). Importantly, for the barriers that do not drown, interiors are lower and narrower than barriers not scoured by outwash (Table 1). The slow recovery of barrier interiors following outwash events in our model simulations is

285 consistent with observations that show persistence of washout features for years to decades 286 (e.g., Himmelstein & Rodriguez, 2025; Over & Sherwood, 2025). 287 Dune gap recovery in our model is influenced by the natural dune growth rate (here, simulated 288 by a low and slightly higher rate) and the degree to which washout is incorporated in the 289 shoreface. We find that when more washout remains on the shoreface, or when dunes grow 290 faster, barriers are less likely to drown (Table 1). More washout remaining nearshore also leads 291 to wider beaches that limit landward shoreline migration (Figure 3a,c), allowing dunes time to 292 regrow (Figure 3b,d). 293 This model incorporates processes relevant for understanding outwash impacts to barrier 294 evolution, but does not resolve all processes that may alter barrier dynamics. In our model, 295 dunes grow every model year but, in reality, dune growth depends on physical and biological 296 conditions (Moore et al., 2024), and washout sites are slower to revegetate (Over & Sherwood, 297 2025). Barriers with lower dunes and interiors are more vulnerable to subsequent outwash 298 events but less vulnerable to SLR because overwash builds elevation (Anarde et al., 2024a). 299 Additionally, although wide beaches may limit overtopping of dunes (Ruggiero et al., 2004; 300 Stockdon et al., 2006), beach width does not influence overwash flux in our model. Inclusion of 301 this dynamic would reduce the frequency of overwashing storms, allowing dunes to recover 302 sooner but leading to less overwash and lower island interiors. Importantly, low and narrow 303 barriers with tall dunes are more vulnerable to drowning from SLR (e.g., Anarde et al., 2024a; 304 Magliocca et al., 2011; Reeves et al., 2021). For simulations longer than 100 years, or for higher 305 rates of SLR, mechanisms that enhance the recovery of dune gaps are likely to enhance barrier 306 vulnerability to drowning from SLR. 307 Changes in overwash or outwash storm climatology (intensity, duration, and frequency) could 308 alter the balance between recovery of dune gaps and the barrier interior, and therefore 309 influence barrier vulnerability. More intense outwashing storms (higher bay-side water levels or 310 longer durations) would increase erosion of the barrier interior while potentially providing 311 more washout sediment to the nearshore. This would make barriers less vulnerable to future 312 outwash events, but potentially more vulnerable to drowning of the back-barrier from SLR via 313 reductions in overwash as dune gaps close. An increase in frequency of outwash events will

likely also enhance vulnerability for the same reasons. Alternatively, an increase in the intensity or frequency of overwashing storms would enhance recovery of the barrier interior while keeping dune gaps low and wide, enhancing vulnerability to future outwash events. Breaches created by outwash may provide an additional mechanism for inlet formation, due to the substantial scouring of the barrier interior and channelization of dune gaps (e.g., Velasquez Montoya et al., 2018), a process not currently incorporated in barrier models (e.g., Nienhuis & Lorenzo-Trueba, 2019). Our simulations focus on a single, 500-m long barrier segment, but barrier systems are inherently more complex. Varying processes may act on different alongshore segments, altering the evolution of the barrier (Anarde et al., 2024b; Hall et al., 1990; Sherwood et al., 2023; Wright et al., 1970). Humans also introduce complexity in recovery timescales by artificially rebuilding dunes and closing gaps to protect infrastructure (Bezzi et al., 2009; Feagin, 2005, 2013; Nordstrom, 2021; Nordstrom & Jackson, 2013). Gayes (1991) found that beach nourishment following Hurricane Hugo expedited infilling of washout channels, which extended into the upper shoreface. Future modifications to the model will include these processes to better understand the role of outwash in barrier evolution. Collectively, these factors that influence dune and barrier recovery – including variability in natural dune growth rate, the degree to which washout is incorporated in the shoreface, and storm climatology – make it difficult to assess the future vulnerability of barriers that experience outwash. Nonetheless, a single outwash event alters the evolution of the barriers in our simulations for decades. Models that do not include outwash are missing a key erosive process that influences the vulnerability of barriers to subsequent storm impacts and SLR, as well as important feedbacks between outwash, dune dynamics, and overwash.

#### **Acknowledgments**

314

315

316

317

318

319

320

321

322

323

324

325

326

327

328

329

330

331

332

333

334

335

336

337

338

339

340

341

This work was supported by the Gulf Research Program Early-Career Research Fellowship (2000013691-2022). We thank the team at the Community Surface Dynamics Modeling System, specifically Eric Hutton, for support in developing CASCADE. We also thank the United States Geological Survey at Woods Hole, MA for collecting post-storm data from Hurricane Dorian.

### **Open Research**

342	The data on which this article is based is available from Anarde et al. (2023) and Reeves et al.
343	(2022). The CASCADE software is available from Anarde, Reeves, et al. (2024). Pre- and post-
344	storm digital elevation maps can be downloaded using the NOAA Data Access Viewer.
345	Conflict of Interest Disclosure
346	The authors declare there are no conflicts of interest for this manuscript.

348	References
349	Anarde, K., Figlus, J., Sous, D., & Tissier, M. (2020). Transformation of Infragravity Waves during
350	Hurricane Overwash. Journal of Marine Science and Engineering, 8(8), 545.
351	https://doi.org/10.3390/jmse8080545
352	Anarde, K. A., Moore, L. J., Murray, A. B., & Reeves, I. R. B. (2023). Simulations for "the future of
353	developed barrier systems—Part I & Part II" [Dataset]. Figshare.
354	https://doi.org/10.6084/m9.figshare.22295413
355	Anarde, K. A., Moore, L. J., Murray, A. B., & Reeves, I. R. B. (2024a). The Future of Developed
356	Barrier Systems: 1. Pathways Toward Uninhabitability, Drowning, and Rebound. Earth's
357	Future, 12(4), e2023EF003672. https://doi.org/10.1029/2023EF003672
358	Anarde, K. A., Moore, L. J., Murray, A. B., & Reeves, I. R. B. (2024b). The Future of Developed
359	Barrier Systems: 2. Alongshore Complexities and Emergent Climate Change Dynamics.
360	Earth's Future, 12(4), e2023EF004200. https://doi.org/10.1029/2023EF004200
361	Anarde, K. A., Reeves, I. R. B., Hutton, E., Williams, Z., Murray, A. B., & Moore, L. J. (2024). UNC-
362	CECL/CASCADE: Release for Earth's Future Publications: The future of developed barrier
363	systems - Parts I & II (Version v1.0.0) [Computer software]. Zenodo.
364	https://doi.org/10.5281/ZENODO.10655831
365	Ashton, A. D., & Ortiz, A. C. (2011). Overwash controls coastal barrier response to sea-level rise.
366	In The Proceedings of the Coastal Sediments 2011 (pp. 230–243). World Scientific
367	Publishing Company. https://doi.org/10.1142/9789814355537 0018
368	Bezzi, A., Fontolan, G., Nordstrom, K. F., Carrer, D., & Jackson, N. L. (2009). Beach Nourishment
369	and Foredune Restoration: Practices and Constraints along the Venetian Shoreline, Italy.
370	Journal of Coastal Research, 56, 287–291. http://www.jstor.org/stable/25737583
371	Bush, D. M., & Pilkey, O. H. (1994). Mitigation of Hurricane Property Damage on Barrier Islands:
372	A Geological View. Journal of Coastal Research, Special Issue No. 12: Coastal Hazards,
373	95–111. https://www.jstor.org/stable/25735607

374	Dolan, R., & Godfrey, P. (1973). Effects of Hurricane Ginger on the Barrier Islands of North
375	Carolina. GSA Bulletin, 84(4), 1329–1334. https://doi.org/10.1130/0016-
376	7606(1973)84%3C1329:EOHGOT%3E2.0.CO;2
377	Donnelly, C., Kraus, N., & Larson, M. (2006). State of Knowledge on Measurement and Modeling
378	of Coastal Overwash. Journal of Coastal Research, 22(4):965–991. Publisher: Coastal
379	Education & Research Foundation, Inc. <a href="https://www.jstor.org/stable/4300354">https://www.jstor.org/stable/4300354</a>
380	Durán, O., & Moore, L. J. (2013). Vegetation controls on the maximum size of coastal dunes.
381	Proceedings of the National Academy of Sciences, 110(43), 17217–17222.
382	https://doi.org/10.1073/pnas.1307580110
383	Durán Vinent, O., & Moore, L. J. (2015). Barrier island bistability induced by biophysical
384	interactions. Nature Climate Change, 5(2), 158–162.
385	https://doi.org/10.1038/nclimate2474
386	Feagin, R. (2013). Foredune Restoration Before and After Hurricanes: Inevitable Destruction,
387	Certain Reconstruction. In M. L. Martínez, J. B. Gallego-Fernández, & P. A. Hesp (Eds.),
388	Restoration of Coastal Dunes (pp. 93–103). Springer. https://doi.org/10.1007/978-3-
389	<u>642-33445-0 6</u>
390	Feagin, R. A. (2005). Artificial Dunes Created to Protect Property on Galveston Island, Texas: The
391	Lessons Learned. Ecological Restoration, 23(2), 89–94.
392	https://doi.org/10.3368/er.23.2.89
393	French, J., Payo, A., Murray, B., Orford, J., Eliot, M., & Cowell, P. (2016). Appropriate complexity
394	for the prediction of coastal and estuarine geomorphic behaviour at decadal to
395	centennial scales. Geomorphology, 256, 3–16.
396	https://doi.org/10.1016/j.geomorph.2015.10.005
397	Gayes, P. T. (1991). Post-Hurricane Hugo Nearshore Side Scan Sonar Survey; Myrtle Beach to
398	Folly Beach, South Carolina. Journal of Coastal Research, Special Issue No. 8. Impacts of
399	Hurricane Hugo: September 10-22, 18. https://www.jstor.org/stable/25735410

400	Goff, J. A., Allison, M. A., & Gulick, S. P. S. (2010). Offshore transport of sediment during
401	cyclonic storms: Hurricane Ike (2008), Texas Gulf Coast, USA. <i>Geology</i> , 38(4), 351–354.
402	https://doi.org/10.1130/G30632.1
403	Goff, J. A., Swartz, J. M., Gulick, S. P. S., Dawson, C. N., & de Alegria-Arzaburu, A. R. (2019). An
404	outflow event on the left side of Hurricane Harvey: Erosion of barrier sand and seaward
405	transport through Aransas Pass, Texas. Geomorphology, 334, 44–57.
406	https://doi.org/10.1016/j.geomorph.2019.02.038
407	Hall, M. J., Young, R. S., Thieler, E. R., Priddy, R. D., & Pilkey, O. H. (1990). Shoreline Response to
408	Hurricane Hugo. Journal of Coastal Research, 6(1), 211–221.
409	https://www.jstor.org/stable/4297660
410	Hayes, M. O. (1967). Hurricanes as Geological Agents: Case studies of Hurricanes Carla, 1961,
411	and Cindy, 1963. University of Texas at Austin. Bureau of Economic Geology, 56.
412	http://dx.doi.org/10.26153/tsw/4849
413	Hesp, P. A. (1989). A review of biological and geomorphological processes involved in the
414	initiation and development of incipient foredunes. Proceedings of the Royal Society of
415	Edinburgh, Section B: Biological Sciences, 96, 181–201.
416	https://doi.org/10.1017/S0269727000010927
417	Himmelstein, J. D., & Rodriguez, A. B. (2025). Washout Versus Washover: Distinct Trajectories
418	of Barrier Reshaping. Journal of Geophysical Research: Earth Surface, 130(4),
419	e2024JF008047. https://doi.org/10.1029/2024JF008047
420	Houser, C., Wernette, P., Rentschlar, E., Jones, H., Hammond, B., & Trimble, S. (2015). Post-
421	storm beach and dune recovery: Implications for barrier island resilience.
422	Geomorphology, 234, 54-63. https://doi.org/10.1016/j.geomorph.2014.12.044
423	Kochel, R. C., & Dolan, R. (1986). The Role of Overwash on a Mid-Atlantic Coast Barrier Island.
424	The Journal of Geology, 94(6). https://doi.org/10.1086/629096

125	Leatherman, S. P. (1979). Migration of Assateague Island, Maryland, by inlet and overwash
126	processes. Geology, 7(2), 104–107. https://doi.org/10.1130/0091-
127	7613(1979)7<104:MOAIMB>2.0.CO;2
128	Lennon, G. (1991). The Nature and Causes of Hurricane-Induced Ebb Scour Channels on a
129	Developed Shoreline. Journal of Coastal Research, Special Issue No. 8. Impacts of
130	Hurricane Hugo: September 10-22, 237–248. https://www.jstor.org/stable/25735418
131	Lorenzo-Trueba, J., & Ashton, A. D. (2014). Rollover, drowning, and discontinuous retreat:
132	Distinct modes of barrier response to sea-level rise arising from a simple
133	morphodynamic model. Journal of Geophysical Research: Earth Surface, 119, 779–801.
134	https://doi.org/10.1002/2013JF002941
135	Magliocca, N. R., McNamara, D. E., & Murray, A. B. (2011). Long-Term, Large-Scale
136	Morphodynamic Effects of Artificial Dune Construction along a Barrier Island Coastline.
137	Journal of Coastal Research, 27(5), 918–930. https://doi.org/10.2112/JCOASTRES-D-10-
138	<u>00088.1</u>
139	Mariotti, G., & Hein, C. J. (2022). Lag in response of coastal barrier-island retreat to sea-level
139 140	Mariotti, G., & Hein, C. J. (2022). Lag in response of coastal barrier-island retreat to sea-level rise. <i>Nature Geoscience</i> , <i>15</i> (8), 633-638. <a href="https://doi.org/10.1038/s41561-022-00980-9">https://doi.org/10.1038/s41561-022-00980-9</a>
140 141	rise. <i>Nature Geoscience</i> , 15(8), 633-638. https://doi.org/10.1038/s41561-022-00980-9
140 141 142	rise. <i>Nature Geoscience</i> , <i>15</i> (8), 633-638. <a href="https://doi.org/10.1038/s41561-022-00980-9">https://doi.org/10.1038/s41561-022-00980-9</a> Moore, L. J., List, J. H., Williams, S. J., & Stolper, D. (2010). Complexities in barrier island
140	rise. <i>Nature Geoscience</i> , <i>15</i> (8), 633-638. <a href="https://doi.org/10.1038/s41561-022-00980-9">https://doi.org/10.1038/s41561-022-00980-9</a> Moore, L. J., List, J. H., Williams, S. J., & Stolper, D. (2010). Complexities in barrier island response to sea level rise: Insights from numerical model experiments, North Carolina
140 141 142 143	rise. <i>Nature Geoscience</i> , <i>15</i> (8), 633-638. <a href="https://doi.org/10.1038/s41561-022-00980-9">https://doi.org/10.1038/s41561-022-00980-9</a> Moore, L. J., List, J. H., Williams, S. J., & Stolper, D. (2010). Complexities in barrier island response to sea level rise: Insights from numerical model experiments, North Carolina Outer Banks. <i>Journal of Geophysical Research</i> , <i>115</i> (F3), F03004.
140 141 142 143 144	rise. <i>Nature Geoscience</i> , <i>15</i> (8), 633-638. <a href="https://doi.org/10.1038/s41561-022-00980-9">https://doi.org/10.1038/s41561-022-00980-9</a> Moore, L. J., List, J. H., Williams, S. J., & Stolper, D. (2010). Complexities in barrier island response to sea level rise: Insights from numerical model experiments, North Carolina Outer Banks. <i>Journal of Geophysical Research</i> , <i>115</i> (F3), F03004. <a href="https://doi.org/10.1029/2009JF001299">https://doi.org/10.1029/2009JF001299</a>
140 141 142 143 144	rise. <i>Nature Geoscience</i> , <i>15</i> (8), 633-638.https://doi.org/10.1038/s41561-022-00980-9  Moore, L. J., List, J. H., Williams, S. J., & Stolper, D. (2010). Complexities in barrier island response to sea level rise: Insights from numerical model experiments, North Carolina Outer Banks. <i>Journal of Geophysical Research</i> , <i>115</i> (F3), F03004. https://doi.org/10.1029/2009JF001299  Murray, A. B., & Paola, C. (1994). A cellular model of braided rivers. <i>Nature</i> , <i>371</i> (6492), 54–57.
140 141 142 143 144 145	rise. <i>Nature Geoscience</i> , <i>15</i> (8), 633-638. <a href="https://doi.org/10.1038/s41561-022-00980-9">https://doi.org/10.1038/s41561-022-00980-9</a> Moore, L. J., List, J. H., Williams, S. J., & Stolper, D. (2010). Complexities in barrier island response to sea level rise: Insights from numerical model experiments, North Carolina Outer Banks. <i>Journal of Geophysical Research</i> , <i>115</i> (F3), F03004. <a href="https://doi.org/10.1029/2009JF001299">https://doi.org/10.1029/2009JF001299</a> Murray, A. B., & Paola, C. (1994). A cellular model of braided rivers. <i>Nature</i> , <i>371</i> (6492), 54–57. <a href="https://doi.org/10.1038/371054a0">https://doi.org/10.1038/371054a0</a>

450	Nienhuis, J. H., & Lorenzo-Trueba, J. (2019). Simulating barrier island response to sea level rise
451	with the barrier island and inlet environment (BRIE) model v1.0. Geoscientific Model
452	Development, 12(9), 4013-4030. https://doi.org/10.5194/gmd-12-4013-2019
453	Nordstrom, K. F. (2021). Dune Building Practices and Impacts. In Beach and Dune Restoration
454	(pp. 65-87). Cambridge University Press. <a href="https://doi.org/10.1017/9781108866453.004">https://doi.org/10.1017/9781108866453.004</a>
455	Nordstrom, K. F., & Jackson, N. L. (2013). Foredune Restoration in Urban Settings. In M. L.
456	Martínez, J. B. Gallego-Fernández, & P. A. Hesp (Eds.), Restoration of Coastal Dunes (pp.
457	17–31). Springer. <a href="https://doi.org/10.1007/978-3-642-33445-0">https://doi.org/10.1007/978-3-642-33445-0</a> 2
458	Over, JS. R., & Sherwood, C. R. (2025). Outwash Events Inhibit Vegetation Recovery and
459	Prolong Coastal Vulnerability. Journal of Geophysical Research: Earth Surface, 130(6),
460	e2024JF008162. https://doi.org/10.1029/2024JF008162
461	Over, JS. R., Brown, J. A., Sherwood, C. R., Hegermiller, C. A., Wernette, P. A., Ritchie, A. C., &
462	Warrick, J. A. (2021). A survey of storm-induced seaward-transport features observed
463	during the 2019 and 2020 hurricane seasons. Shore and Beach, 89(2), 31–40.
464	http://doi.org/10.34237/1008924
465	Parker, G. (1978). Self-formed straight rivers with equilibrium banks and mobile bed. Part 2. The
466	gravel river. Journal of Fluid mechanics, 89(1), pp.127-146.
467	https://doi.org/10.1017/S0022112078002505
468	Reeves, I. R. B., Anarde, K. A., & Moore, L. J. (2022). Record of storm events and associated
469	water levels for the Virginia Coast Reserve, 1980–2013 [Dataset]. Virginia Coast Reserve
470	Long-Term Ecological Research Project Data Publication knb-lter-vcr.352.1. Retrieved
471	from https://www.vcrlter.virginia.educgi-bin/showDataset.cgi?docid=knb-lter-vcr.352.1
472	Reeves, I. R. B., Moore, L. J., Murray, A. B., Anarde, K. A., & Goldstein, E. B. (2021). Dune
473	Dynamics Drive Discontinuous Barrier Retreat. Geophysical Research Letters, 48(13).
474	https://doi.org/10.1029/2021GL092958

475	Ruggiero, P., Holman, R. A., & Beach, R. A. (2004). Wave run-up on a high-energy dissipative
476	beach. Journal of Geophysical Research: Oceans, 109(C6).
477	https://doi.org/10.1029/2003JC002160
478	Sherwood, C. R., Long, J. W., Dickhudt, P. J., Dalyander, P. S., Thompson, D. M., & Plant, N. G.
479	(2014). Inundation of a barrier island (Chandeleur Islands, Louisiana, USA) during a
480	hurricane: Observed water-level gradients and modeled seaward sand transport. Journal
481	of Geophysical Research: Earth Surface, 119(7), 1498–1515.
482	https://doi.org/10.1002/2013JF003069
483	Sherwood, C. R., Ritchie, A. C., Over, J. R., Kranenburg, C. J., Warrick, J. A., Brown, J. A., Wright,
484	C. W., Aretxabaleta, A. L., Zeigler, S. L., Wernette, P. A., Buscombe, D. D., & Hegermiller,
485	C. A. (2023). Sound-Side Inundation and Seaward Erosion of a Barrier Island During
486	Hurricane Landfall. Journal of Geophysical Research: Earth Surface, 128(1).
487	https://doi.org/10.1029/2022JF006934
488	Stockdon, H. F., Holman, R. A., Howd, P. A., & Sallenger, A. H. (2006). Empirical
489	parameterization of setup, swash, and runup. Coastal Engineering, 53(7), 573–588.
490	https://doi.org/10.1016/j.coastaleng.2005.12.005
491	Velasquez Montoya, L., Sciaudone, E. J., Mitasova, H., & Overton, M. F. (2018). Observation and
492	modeling of the evolution of an ephemeral storm-induced inlet: Pea Island Breach,
493	North Carolina, USA. Continental Shelf Research, 156, 55–69.
494	https://doi.org/10.1016/j.csr.2018.02.002
495	Wahl, T., Plant, N. G., & Long, J. W. (2016). Probabilistic assessment of erosion and flooding risk
496	in the northern Gulf of Mexico. Journal of Geophysical Research: Oceans, 121(5), 3029–
497	3043. https://doi.org/10.1002/2015JC011482
498	Warner, J. C., Sherwood, C. R., Hegermiller, C. A., Defne, Z., Zambon, J., He, R., et al. (2025).
499	Numerical Simulation of Sound-Side Barrier-Island Inundation and Breaching During
500	Hurricane Dorian (2019). Journal of Geophysical Research: Earth Surface, 130(6),
501	e2025JF008309. https://doi.org/10.1029/2025JF008309

502	Westerink, J. J., Luettich, R. A., Baptists, A. M., Scheffner, N. W., & Farrar, P. (1992). Tide and
503	storm surge predictions using finite element model. Journal of hydraulic Engineering,
504	118(10), 1373-1390. https://doi.org/10.1061/(ASCE)0733-9429(1992)118:10(1373)
505	Wright, L. D., Swaye, F. J., & Coleman, J. M. (1970). Effects of Hurricane Camille on the
506	landscape of the Breton-Chandeleur Island Chain and the eastern portion of the lower
507	Mississippi Delta (Technical 76; p. 25). Coastal Studies Institute, Louisiana State
508	University.
509	Zarnetske, P. L., Hacker, S. D., Seabloom, E. W., Ruggiero, P., Killian, J. R., Maddux, T. B., & Cox
510	D. (2012). Biophysical feedback mediates effects of invasive grasses on coastal dune
511	shape. <i>Ecology, 93</i> (6), 1439–1450. <a href="https://doi.org/10.1890/11-1112.1">https://doi.org/10.1890/11-1112.1</a>
512	

513	References From the Supporting Information
514	Anarde, K. A., Moore, L. J., Murray, A. B., & Reeves, I. R. B. (2023). Simulations for "the future of
515	developed barrier systems—Part I & Part II" [Dataset]. Figshare.
516	https://doi.org/10.6084/m9.figshare.22295413
517	Bruun, P. (1962). Sea-level rise as a cause of shore erosion. Journal of the Waterways and
518	Harbors Division, 88(1), 117–132. <a href="https://doi.org/10.1061/JWHEAU.0000252">https://doi.org/10.1061/JWHEAU.0000252</a>
519	Bruun, P. (1988). The Bruun Rule of Erosion by Sea-Level Rise: A Discussion on Large-Scale Two-
520	and Three-Dimensional Usages. Journal of Coastal Research, 4(4), 627–648.
521	https://www.jstor.org/stable/4297466
522	French, J., Payo, A., Murray, B., Orford, J., Eliot, M., & Cowell, P. (2016). Appropriate complexity
523	for the prediction of coastal and estuarine geomorphic behaviour at decadal to
524	centennial scales. Geomorphology, 256, 3–16.
525	https://doi.org/10.1016/j.geomorph.2015.10.005
526	Lorenzo-Trueba, J., & Ashton, A. D. (2014). Rollover, drowning, and discontinuous retreat:
527	Distinct modes of barrier response to sea-level rise arising from a simple
528	morphodynamic model. Journal of Geophysical Research: Earth Surface, 119, 779–801.
529	https://doi.org/10.1002/2013JF002941
530	Murray, A. B. (2003). Contrasting the Goals, Strategies, and Predictions Associated with
531	Simplified Numerical Models and Detailed Simulations. In Prediction in Geomorphology
532	(pp. 151–165). American Geophysical Union (AGU). <a href="https://doi.org/10.1029/135GM11">https://doi.org/10.1029/135GM11</a>
533	Murray, A. B., & Paola, C. (1994). A cellular model of braided rivers. <i>Nature</i> , <i>371</i> (6492), 54–57.
534	https://doi.org/10.1038/371054a0
535	Murray, A. B., & Paola, C. (1997). Properties of a cellular braided-stream model. Earth Surface
536	Properties and Landforms, 22(11), 1001–1025. <a href="https://doi.org/10.1002/(SICI)1096-">https://doi.org/10.1002/(SICI)1096-</a>
537	9837(199711)22:11%3C1001::AID-ESP798%3E3.0.CO;2-O

538	Reeves, I. R. B., Moore, L. J., Murray, A. B., Anarde, K. A., & Goldstein, E. B. (2021). Dune
539	Dynamics Drive Discontinuous Barrier Retreat. Geophysical Research Letters, 48(13).
540	https://doi.org/10.1029/2021GL092958
541	Sherwood, C. R., Ritchie, A. C., Over, J. R., Kranenburg, C. J., Warrick, J. A., Brown, J. A., Wright,
542	C. W., Aretxabaleta, A. L., Zeigler, S. L., Wernette, P. A., Buscombe, D. D., & Hegermiller
543	C. A. (2023). Sound-Side Inundation and Seaward Erosion of a Barrier Island During
544	Hurricane Landfall. Journal of Geophysical Research: Earth Surface, 128(1).
545	https://doi.org/10.1029/2022JF006934
546	

### Geophysical Research Letters

### Supporting Information for

# Barrier vulnerability following outwash: a balance of overwash and dune gap recovery

A. G. Van Blunk<sup>1</sup>, K. A. Anarde<sup>1\*</sup>, A. B. Murray<sup>2</sup>, L. J. Moore<sup>3</sup>, C. R. Sherwood<sup>4</sup>

<sup>1</sup>Department of Civil, Construction, and Environmental Engineering, North Carolina State University, Raleigh, NC, USA.

<sup>2</sup>Division of Earth and Climate Sciences, Nicholas School of the Environment, Duke University, Durham, NC, USA.

<sup>3</sup>Department of Earth, Marine and Environmental Sciences, University of North Carolina at Chapel Hill, Chapel Hill, NC, USA.

<sup>4</sup>Woods Hole Coastal and Marine Science Center, U.S. Geological Survey, Woods Hole, MA, USA.

\*Corresponding author: Katherine Anarde (<u>kanarde@ncsu.edu</u>)

#### Contents of this file

Text S1 Figures S1 to S6 Table S1

### Introduction

The supporting text gives more detail on how we developed the "Outwasher" module from previously implemented flow, sediment transport, and shoreface and dune dynamics equations (Anarde et al., 2023; Murray & Paola, 1994, 1997; Reeves et al., 2021). Supporting figures show the steps taken to convert elevation data into gridded array data, the hydrograph used to simulate outwash storms, an example of how flow is initially distributed during an outwash event, results from the three configurations used for tuning sediment transport parameters, and overwash and barrier evolution results for the high (r=0.35) dune growth rate. The supporting table gives the tuned sediment transport parameters for each configuration and the final values used for model testing and results.

#### Text S1.

Here, we provide more details on the outwash module dynamics. Section 1 describes how we used real-world DEM data to initialize our domain. Section 2 describes the flow routing rules, highlighting important equations. Section 3 defines sediment transport equations and tuning methods. Section 4 describes how outwash events are implemented in the model and the different scenarios tested. Finally, Section 5 explains how the variables were calculated for the results.

#### 1. Domains

CASCADE uses real-world elevation data to create the model domains, which requires manipulation in a GIS software. We started with a Digital Elevation Model (DEM) downloaded from the National Oceanic and Atmospheric Administration's (NOAA) Data Access Viewer. First, since the datum in Barrier3D is mean high water (MHW), we convert the NOAA DEM from meters NAVD88 to meters MHW using the NOAA tide gauge in Beaufort, NC at the Duke Marine Lab station. MHW is currently 0.36 m above NAVD88. Next, we set all bay (water) cells in the DEM to -3 m MHW, which coincides with the initial bay elevation in Barrier3D. This is also the minimum elevation allowed in the domain. Although the DEM has a resolution of 1 m x 1 m, elevations are averaged to a 10 m x 10 m resolution because this is the cell size used in Barrier3D. Once these steps are complete, we download the point elevation data for reconstruction as an array in Python. Figure S1 shows an example of some of these conversion steps. Once in CASCADE, the domain is broken up into an interior and dune domain. In Outwasher, we recombine the interior and dune domains, plus add a beach domain. This is because we apply the same flow and sediment routing rules to the entire domain whereas Barrier3D applies separate rules to each domain.

### 2. Flow Routing Rules

Here, we describe the rules in more detail, stepping through the Outwasher time steps. As an "appropriate complexity" (French et al., 2016) model, the rules implemented

in Outwasher are meant to simulate only the most important processes observed during outwash events (Murray, 2003).

### 2.1 Initiating Flow

Outwash can only occur when the bay-side water levels (Figure S2) exceed the dune gap elevations. The hourly hydrograph (red points, Figure S2) was generated using ADCIRC (Sherwood et al., 2023) but modified in Python to make the time-step increments every six minutes (blue and red points, Figure S2). This ensures the model does not have a large spike in bay-side water levels.

If the bay-side water level exceeds the dune gaps, we then check to ensure there is a hydraulic connection between the bay and dune gaps because occasionally, the dune gaps are lower than the barrier interior. Therefore, the interior prevents the water from reaching the dunes. This process is shown in Figure S3, where the shaded cells (light grey, dark grey, and black) are all "submerged," meaning their elevations are less than the bay elevation.

We assume that water slopes follow bed slopes, so we identify the cells that lead downhill toward the dune gaps. These are the dark grey cells in Figure S3. We only want to route water over each cell once per time step, so we identify the most landward downhill cells in each column that are not likely to be influenced by cells in adjacent columns (black cells in Figure S3). These become our start cells where we initiate flow.

We apply a conservation of flow rule at the start point cells based on the expected flow through the dune gaps. The discharge at the dune gaps is calculated according to

$$Q_{dune} = h\sqrt{2gh}$$

where h is the water height above the dune gap and g is gravitational acceleration. We sum the discharge at each dune gap cell and evenly distribute it among the start cells.

$$Q_0 = \frac{\sum Q_{dune}}{number\ of\ start\ cells}$$

#### 2.2 Distributing Flow

Once we have an initial discharge at the start cells, we route the flow through the interior, dune gaps, and beach using the cellular flow routing scheme developed by Murray & Paola (1994, 1997) for braided rivers and implemented by Reeves et al. (2021) for overwash:

$$Q_i = \frac{Q_0 * S_i^n}{\sum S_i^n}$$

where the 0 subscript indicates a distributing cell and the i subscript indicates a receiving downstream cell.  $Q_0$  is the discharge at the distributing cell,  $Q_i$  and  $S_i$  are the discharge and slope to the downstream cell, respectively. n is a constant set to 0.5 (consistent with Murray & Paola, 1994, 1997; Reeves et al., 2021). Each cell is connected to its three downstream cells. Water preferentially flows downhill (positive  $S_i$  value), so if there are

uphill and downhill (negative  $S_i$  value) cells, none of the water flows to the uphill ones. If all three slopes are 0, then the flow is divided evenly among the three downstream cells. Lastly, if all slopes are uphill, we distribute more water to the cell with the shallowest slope and less to the cell with the steepest slope. We also follow the modification made by (Reeves et al., 2021) to linearly reduce the discharge distributed uphill based on a maximum uphill slope limit. When a slope exceeds the limit, we do not distribute any water to that cell. Therefore, when all downstream slopes are uphill, we use the following flow routing equation:

$$Q_{i} = \begin{cases} \frac{Q_{0} * |S_{i}|^{-n}}{\sum |S_{i}|^{-n}} * \left(1 - \frac{|S_{i}|}{|S_{max}|}\right), & S_{i} \ge S_{max} \\ 0, & S_{i} < S_{max} \end{cases}$$

noting that  $S_i$  and  $S_{max}$  are negative. This equation is slightly modified for outwash from the version used by (Reeves et al., 2021) because we leave out a term,  $R_{in}$ , which was based on the overwash regime.

### 3. Tuning Sediment Transport

In Outwasher, sediment moves downstream (seaward) or laterally based on sediment transport equations developed by Murray & Paola (1994, 1997) for braided rivers and implemented by Reeves et al. (2021) for overwash. These equations have numerous variables that can be changed to better represent specific morphological behaviors. To create accurate outwash events, we tuned these parameters using real-world data from Hurricane Dorian (2019). Below, we describe the three domains used for model tuning, then explain the sediment transport process in more detail in the following sections.

The pre-storm, post-storm, and elevation change figures for the three configurations we used for tuning are shown in Figure S4. Each domain has unique morphological outwash features and erosional volumes, which we want to capture in the model. However, due to the nature of our reduced-complexity approach, we know that we will not be able to capture the exact morphology or volume changes observed. Volume changes are calculated by subtracting the post-storm from the pre-storm to get a change in elevation, then multiplying by the cell length and width to get volume. In Figure S4, red shows erosion and blue shows accretion. For configurations 1 and 2, the erosional volume that we try to match is outlined by the boxes. For configuration 3, we use the back barrier and dunes (from cross-shore position 0 to the black line) because channels form throughout the entire domain. We also show the best modeled result below each observed result (Figure S4). We do not need to specify a box for these volumes because we only get erosion at the channels; therefore, we calculate the volumetric erosion for the entire back-barrier and dunes (cross-shore position 0 to the black line). Table S1 provides a summary of the results from our tuning process.

After finding the ideal sediment transport parameters for each configuration (described in more detail below), we average them and test their accuracy on a fourth configuration (Figure S5). The average sediment transport parameters performed well on

the un-tuned configuration. The observed erosion, calculated within the area of the black box (Figure S5), was 55,200 m³ whereas the modeled erosion in the back-barrier and dunes (cross-shore position 0 to the black line) was 44,000 m³. Configurations 1 and 2 both underestimated volumetric erosions, so we are not surprised to see a conservative volumetric erosion for this case as well. Additionally, the model produced similar morphological features. The widest breach occurs on the left side of the domain and all the breaches spread in the back barrier. Although there is an extra channel that forms in the model, it is clear from the observed data that there is a low point in the dunes where the extra breach forms. It is likely that this channel formed due to the model's inability to replicate the initial dune domain. The model only allows two rows of dunes, but the observed pre-storm elevation shows closer to four dune rows, which provides increased resilience against flows. Despite the discrepancies, the results verify that the model can simulate morphological changes caused by outwash events when using the tuned sediment transport parameters.

#### 3.1 Downstream Sediment Transport

We use the sediment transport equations developed by Murray & Paola (1994, 1997) to distribute sediment to downstream cells and laterally. The downstream equation relates the stream power index nonlinearly to sediment transport:

$$Q_{si} = K_i (Q_i(S_i + C))^m$$

$$C = C_r * m \ beach$$

Where  $K_i$  is a sediment transport coefficient,  $Q_i$  and  $S_i$  are as previously defined,  $C_x$  is a constant,  $m\_beach$  is the average beach slope, and m is set to 0.5 following Reeves et al. (2021).  $K_i$  is a tunable parameter, loosely related to porosity, that we set to a maximum possible value without introducing instability in the model. Here, instability means moving too much sediment, thereby changing the sign of  $S_i$  for every time step, creating an oscillating slope. C is a constant that represents the flow momentum and deemphasizes the role of the local slope in determining sediment transport capacity. We tested many combinations of  $K_i$  and  $C_x$  values on all three tuning domains (Figure S4), finding ideal sets for each one (Table S1). We found that smaller beach slopes required much larger  $C_x$  values, making C more uniform compared to  $C_x$ . Therefore, we used the average  $K_i$  and C values (bolded in Table S1), to test the model on the fourth, untuned configuration.

### 3.2 Lateral Sediment Transport

Cells can also transfer sediment to neighbor cells on their left and right. This process is especially important to widen dune gaps during overwash and outwash. We use the lateral transport equation by Murray & Paola (1994, 1997):

$$Q_{SL} = K_L S_L Q_{Sout}$$

where  $Q_{SL}$  is the amount of sediment transported from a lateral-neighbor cell into the cell in question,  $K_L$  is a constant adjusted so that  $Q_{SL}$  is on the order of a few percent of  $Q_{SOUT}$  (the total sediment load out of the cell in question into the three downstream cells), and  $S_L$  is the lateral slope. If  $S_L$  is 0 or negative (uphill), there is no lateral transport and  $Q_{SL}$  is also 0. After testing multiple  $K_L$  values on all three domains, we found that a  $K_L$  of 0.5 produced the best results in every case, so we apply that as a constant value.

### 4. Washout Incorporation into the Shoreface

We assume that the shoreface and beach generally want to maintain an equilibrium shape (Bruun 1962,1988). Storms can erode sediment from the upper shoreface, supplying sediment for overwash events. This causes the shoreface slope to flatten (Bruun 1962, 1988; Lorenzo-Trueba and Ashton 2014). Alternatively, sediment eroded by outwash events may supply the shoreface with sediment, steepening the shoreface slope as described below.

To understand how the fate of washout impacts barrier evolution, we run four scenarios: baseline (no outwash implemented), incorporating 100% of the washout sediment into the shoreface (all sediment remains in barrier system), 50% into the shoreface (some sediment is lost from the barrier system), or 0% into the shoreface (all sediment is lost). When we add sediment to the shoreface, we adjust the shoreline position described by Ashton & Lorenzo-Trueba (2014) and used by Anarde et al. (2023) in the CASCADE framework for shoreface nourishment by humans;

$$x_{s2} = x_{s1} - \frac{2v}{2h_b + d_s}$$

where  $x_{s2}$  is the new shoreline position,  $x_{s1}$  is the original shoreline position,  $h_b$  is the average barrier height, and  $d_s$  is the shoreface depth. This nourishment formulation results in a steeper shoreface slope because it holds the shoreface toe constant while moving the shoreline position seaward. Moving the shoreline seaward creates a "beach" that halts dune migration. As sea levels rise, the new beach erodes rather than the dunes. Dune migration begins again once shoreline erosion causes the beach to erode to a minimum width.

### 5. Variables used in Results

We analyzed a wide range of variables to better understand the impacts of outwash on barrier evolution including tendency to drown, average outwash and overwash sediment fluxes, average dune crest elevation and length of dune gaps, and average final interior elevation, width, and shoreline position for each outwash and dune growth scenario. Each statistic (mean and percent) is calculated for the 100 overwash storm sequences. If the barrier becomes too low in elevation or narrow in width it can drown before the 100-year simulation ends. Hence, the percent drowned statistic represents the number of barriers that drown for the 100 different storm sequences.

The storm sediment fluxes and dune morphology variables are averaged twice. As stated previously, each ocean-side storm series is simulated for 100 years, or less if the

barrier drowns. The ocean-side storm series contains information for each model year about the number and intensity of storms that occur. None, one, or multiple ocean-side storms may occur each model year, so the total overwash flux is summed to get one value per model year. Additionally, each model year contains an outwash flux (during outwash years), dune crest elevation (averaged in the alongshore), and the total length of dune gaps – here calculated as the number of dune cells (10-m long) that fall below or equal to 0.075 m in height, which is the height at which dunes are initialized in the model (above the berm) if they are completely eroded at the end of a model year. First, we take the average over the simulation time frame, which gives one value of overwash flux, outwash flux, dune crest elevation, and total length of dune gaps for one storm sequence. We then average the values for all 100 storm sequences.

For the barrier interior elevation (above 0 MHW) and interior width, we only look at the final model domain for the simulations that do not drown (i.e., at year 100). We take the average width and elevation of this domain to get a single number for each storm sequence, then average the results for all 100 storm sequences.

Lastly, the final shoreline position is the net migration of a barrier, averaged for all non-drowning storm sequences. In this model, the barrier migrates as a whole, so each cell (at the ocean-interface, Figure S6 b-e) in the alongshore has the same shoreline position. In this way, the barrier evolution variables are representative of a simulation end state that can be directly compared to the baseline scenario.

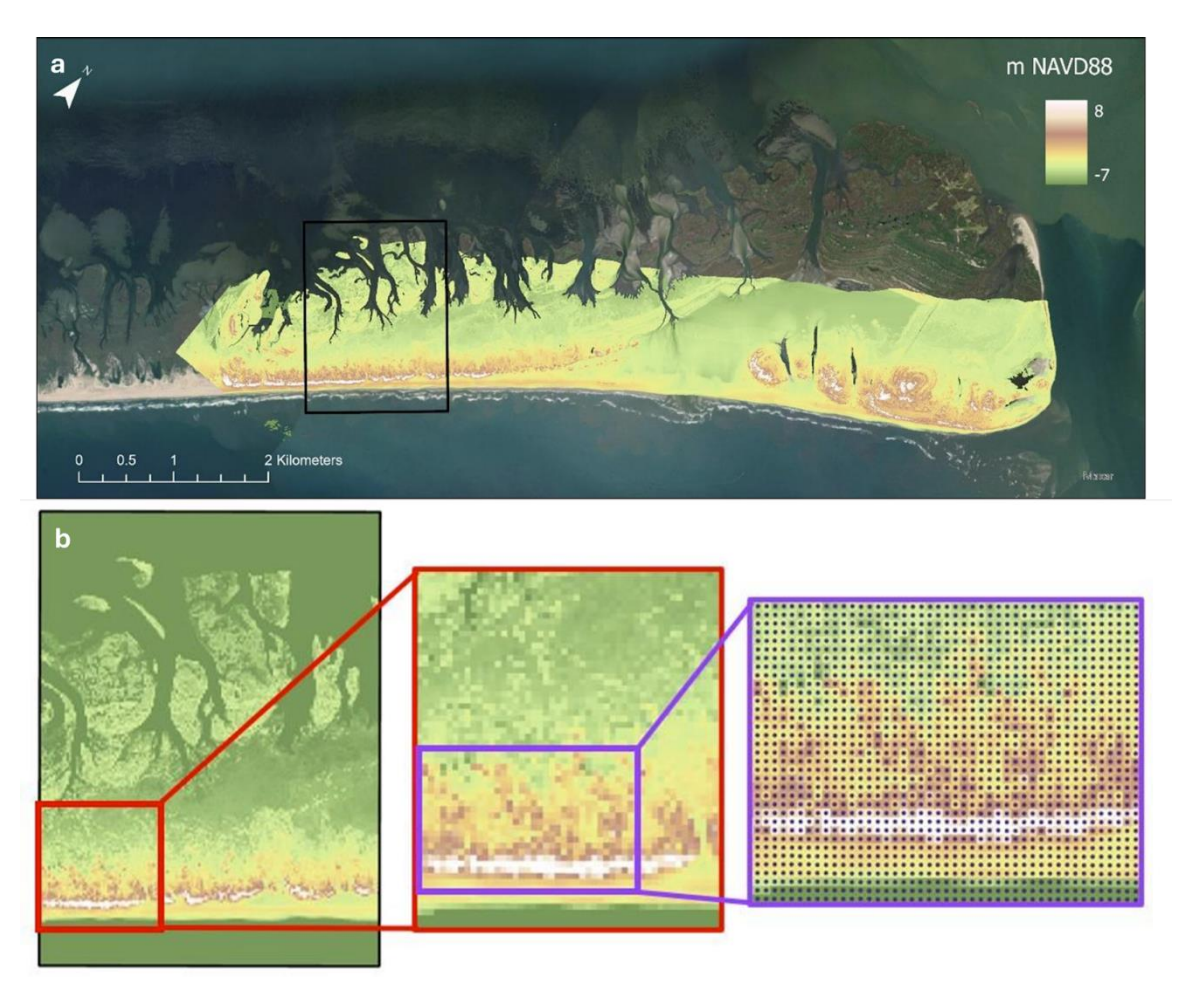


**Figure S1. (a)** The pre-storm DEM post-Hurricane Florence (2017) and **(b)** an example of the steps taken to resample the original raster from 1 m<sup>2</sup> resolution to 100 m<sup>2</sup> resolution (red box). After resampling, we convert raster cells to data points representing elevation (purple box).

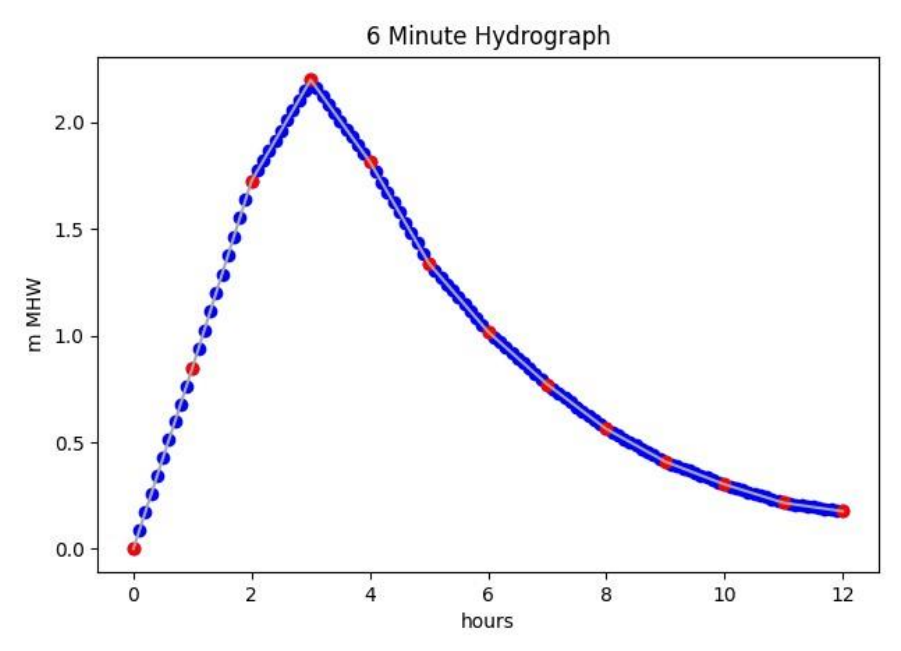


**Figure S2.** The hourly (red points) ADCIRC-generated bay levels from Hurricane Dorian (Sherwood et al., 2023) converted from m MSL to m MHW. We sub-sample at 6-min intervals (blue points) to improve representation of morphological change.

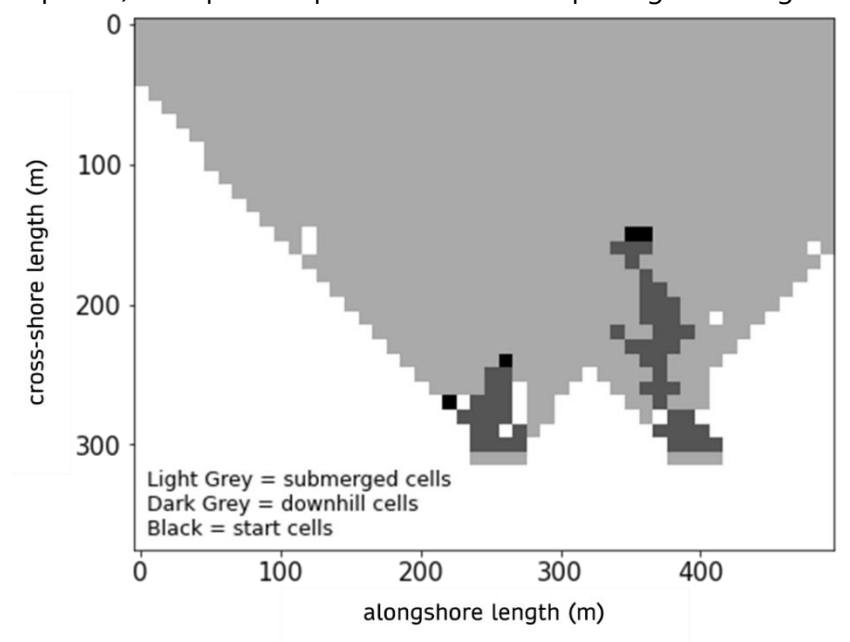


**Figure S3.** Example flow routing array for a single model sub-time-step, with the submerged cells in light grey, downhill cells in dark grey, and the start cells in black (i.e., where flow routing is initiated).

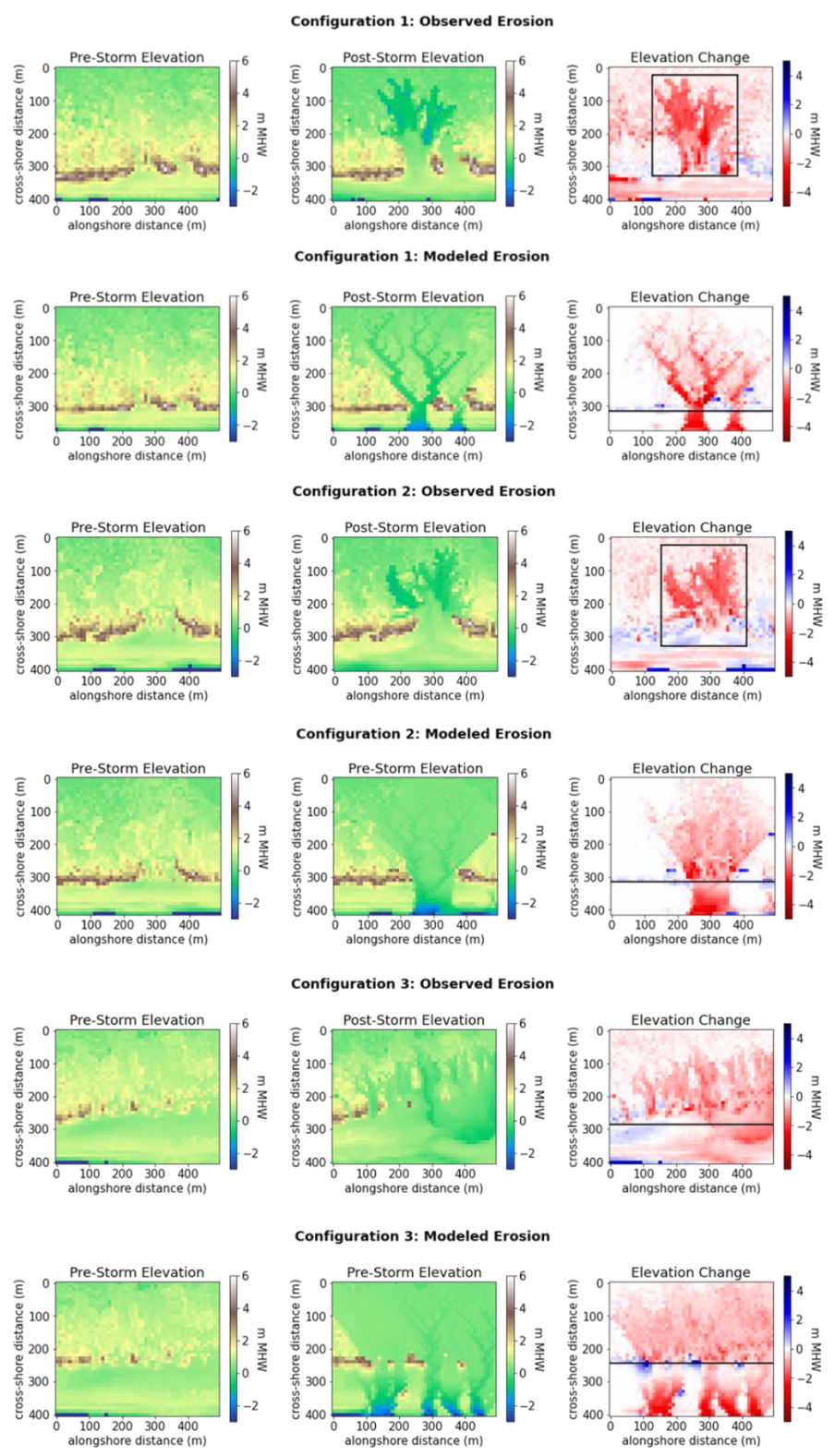


**Figure S4.** Observed and modeled erosion for the three tuning configurations. For configurations 1 and 2, the erosional volume that we try to match is outlined by the boxes. For configuration 3, we use the back barrier and dunes (from cross-shore position 0 to the black line) because channels form throughout the entire domain.

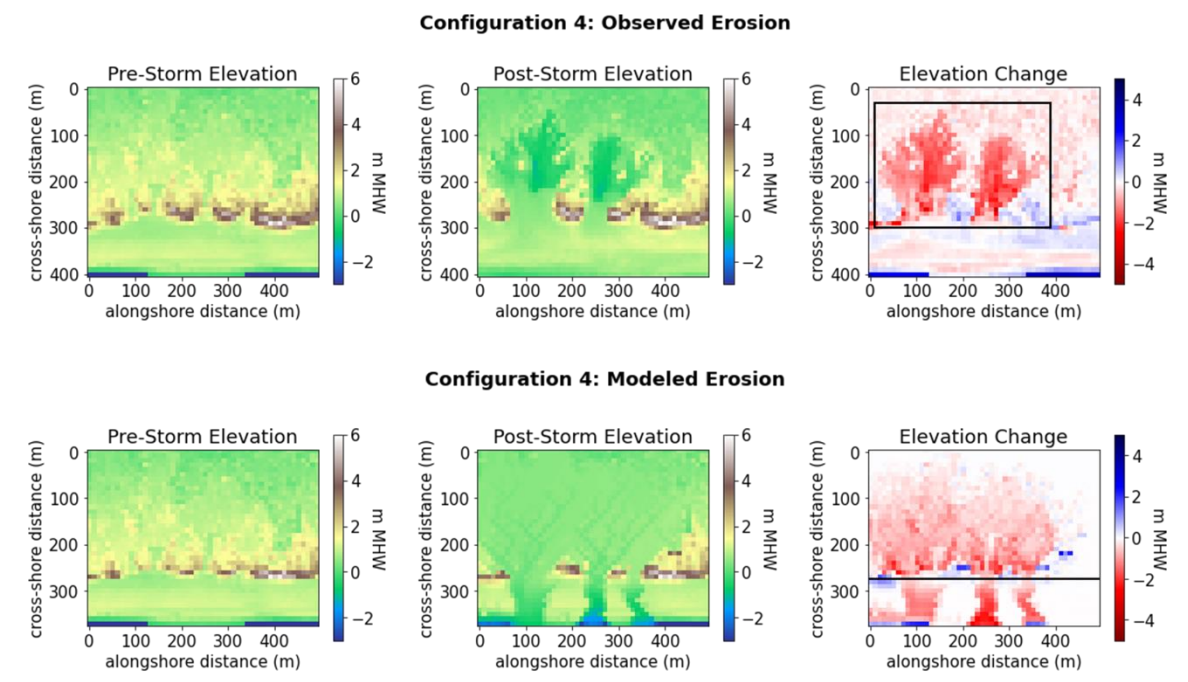
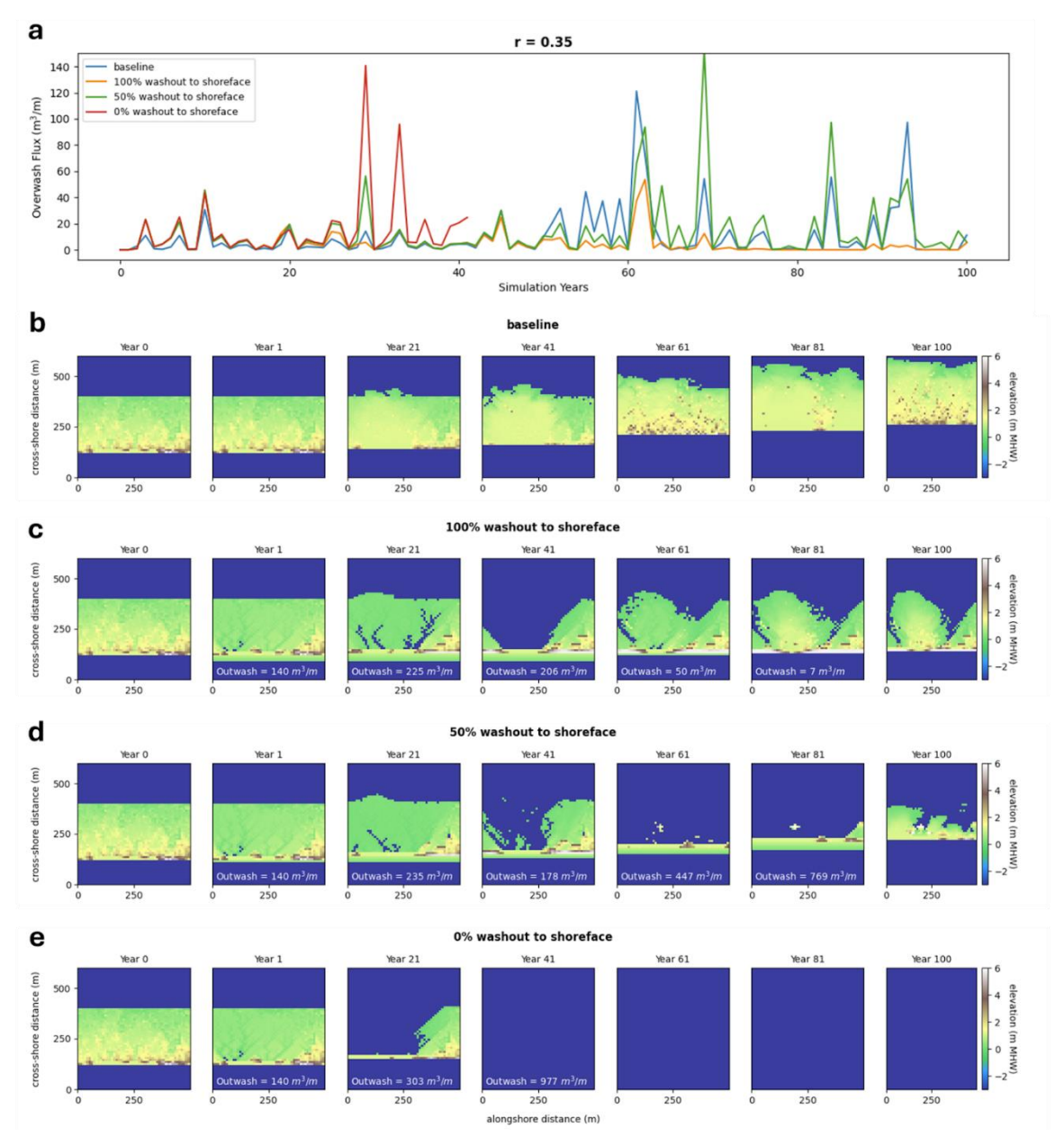


Figure S5. Configuration 4 observed and modeled erosion.



**Figure S6. a)** Overwash flux and **b-e)** barrier island elevation plan views for the high dune growth rate scenario (r=0.35) for the same overwash storm sequence in Figures 2-3. Plan views are limited to outwash events (every 20 years) plus the initial (year 0) and final (year 100) elevations. Outwash fluxes are included on the plan views when relevant.

Configuration	m_beach	Ki	C <sub>x</sub>	C (m_beach*C <sub>x</sub> )	Observed Erosion (m³)	Modeled Erosion (m³)	Total Outwash Volume (m³)
1	0.03	9.50E-03	0.45	0.0135	58,300	42,200	59,700
2	0.013	8.50E-03	1.05	0.01365	45,100	44,600	67,100
3	0.002	8.25E-03	6.5	0.013	58,900	60,900	119,800
	Averages	8.75E-03	2.667	0.0134			

**Table S1.** Tuned sediment transport parameters ( $K_i$  and  $C_x$ ) for the three calibration domains.